# $Ca^{2+}$ Binding to Calbindin $D_{9k}$ Strongly Affects Backbone Dynamics: Measurements of Exchange Rates of Individual Amide Protons Using $^1H$ NMR†

Sara Linse,* Olle Teleman, and Torbjörn Drakenberg
*Physical Chemistry 2, Chemical Centre, Lund University, P.O. Box 124, S-221 00 Lund, Sweden*
*Received January 3, 1990; Revised Manuscript Received March 23, 1990*

ABSTRACT: One- and two-dimensional $^1H$ NMR have been used to study the backbone dynamics in $Ca^{2+}$-free (apo) and $Ca^{2+}$-loaded ($Ca_2$) calbindin $D_{9k}$ at pH 7.5 and 25 °C. Hydrogen exchange rates of all 71 backbone amide protons (NH's) have been measured for the $Ca_2$ form by both a direct exchange-out experiment and another experiment that measures the transfer of saturation from water protons to amide protons. A large number of NH's are found to be highly protected against exchange with solvent protons. The results for the $Ca_2$ form are related to solvent accessibility and hydrogen bonding obtained in molecular dynamics simulations of calcium-loaded calbindin. The correlation with these parameters is strong within the N-terminal half of calbindin, which is found to be more stable than the C-terminal half. The amide proton exchange in the apo form is much faster than in the $Ca_2$ form and was studied in a series of experiments in which the exchange was quenched after different times by $Ca^{2+}$ addition. This experiment is applicable to all amide hydrogens that exchange slowly in the $Ca_2$ form. For these NH's the effects of $Ca^{2+}$ removal span from a $10^2$-fold decrease to a $10^5$-fold increase of the exchange rate, and the average is a 220-fold increase. The effects on individual NH exchange rates show that the four $\alpha$-helices are almost intact after calcium removal and that the changes in dynamics involve not only the $Ca^{2+}$-binding region. Hydrogen bonds involving backbone NH's in the $Ca^{2+}$ loops appear to be broken or weakened when calbindin releases $Ca^{2+}$, whereas the $\beta$-sheet between the $Ca^{2+}$ loops is found to be present in both the $Ca_2$ and apo forms. Large $Ca^{2+}$-induced effects on NH exchange rates were measured for a few residues at $\alpha$-helix ends far from the two $Ca^{2+}$-binding sites. This may be the result of a change in interhelix angles (or the rate of interhelix angle fluctuations) on calcium binding.

Measurement of hydrogen exchange rates for a protein in the absence and presence of a ligand is a sensitive method for detecting conformational changes on ligand binding. The rate of exchange of backbone amide hydrogens depends on fluctuations that allow contacts between amide protons and solvent molecules. Measurement of these rates thus yields insight into dynamics crucial to protein function. Basic pancreatic trypsin inhibitor (BPTI) has been most extensively studied for amide proton exchange behavior under various conditions (Wagner, 1983; Tüchsen & Woodward, 1985, 1987), and there is an increasing number of proteins subjected to detailed studies [e.g., O'Neil and Sykes (1988), Qiwen et al. (1987), and Haruyama et al. (1989)]. The distribution of exchange rates of individual amide protons along the amino acid sequence of a protein is highly sensitive to conformational changes [reviewed by Woodward et al. (1982)]. Using high-resolution techniques such as NMR[1] spectroscopy, it is possible to determine NH exchange rates throughout the entire protein. Detailed investigations of protein dynamics, stability, ligand binding, and folding kinetics are thus facilitated.

In a number of cases, e.g., hemoglobin (Benson et al., 1972) and *lac* repressor (Ramstein et al., 1979), the effect of ligand binding on the collective exchange of all amide protons in the protein has been measured, by use of UV spectroscopy or tritium labeling. A common picture is that ligand binding retards backbone dynamics, but exceptions do exist (Benson et al., 1972). $^1H$ NMR provides the necessary resolution for more detailed investigations and has, for example, made it possible to study the effect on individual amide protons of peptide binding to calmodulin (Seeholzer et al., 1986, 1989) and of oxidation of cytochrome *c* (Wand et al., 1986).

Calbindin $D_{9k}$ belongs to the calmodulin superfamily (Kretsinger, 1987) of regulatory $Ca^{2+}$-binding proteins that contain one or more pairs of EF-hand $Ca^{2+}$-binding sites (Kretsinger & Nockolds, 1973)—a structural motif enabling cooperative $Ca^{2+}$ binding. The $Ca^{2+}$-induced changes in structure and dynamics form a basis for their regulatory function and constitute a central issue in biophysical studies of EF-hand proteins. Calbindin $D_{9k}$ contains one EF-hand pair and can bind two $Ca^{2+}$ ions with high affinity and cooperativity. The crystal structure of calcium-loaded bovine calbindin $D_{9k}$ (Szebenyi & Moffat, 1986), as schematically outlined in Figure 1, contains four $\alpha$-helices that are connected by loop segments. The first and third loops provide the $Ca^{2+}$ ligands in sites I and II, respectively. A short antiparallel $\beta$-sheet is formed between these loops. Recent $^1H$ NMR studies of $Ca^{2+}$-loaded ($Ca_2$) calbindin (Drakenberg et al., 1989; Kördel et al., 1989) show that there is essentially no difference between solution and crystal structures as regards helical segments and $\beta$-sheet. There is increasing evidence that although $Ca^{2+}$ binding to calbindin markedly affects the stability (Wendt et al., 1988) and dynamics (Skelton et al., 1989), the $Ca^{2+}$-induced conformational changes are relatively small and do not affect the general fold (Skelton et al., 1989; B. Svensson, personal communication).

† This work was supported by the Swedish Natural Science Research Council (K-KU-2545-300). The NMR spectrometer was purchased with generous grants from the Knut and Alice Wallenberg Foundation and the Swedish Council for Planning and Coordination of Research (FRN).

[1] Abbreviations: NMR, nuclear magnetic resonance; COSY, *J*-correlated spectroscopy; NOE, nuclear Overhauser enhancement; NH, backbone amide proton; quin 2, 2-[[2-[bis(carboxymethyl)amino]-5-methylphenoxy]methyl]-6-methoxy-8-[bis(carboxymethyl)amino]-quinoline.

0006-2960/90/0429-5925$02.50/0 

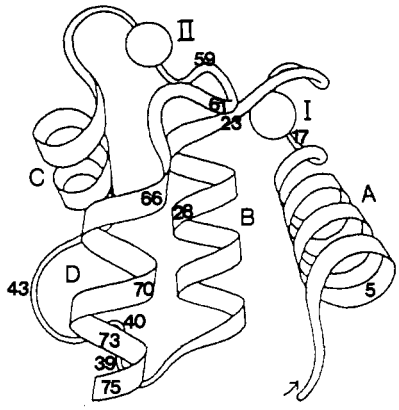


FIGURE 1: Schematic structure of calbindin $D_{9k}$. Letters refer to $\alpha$-helices, Roman numbers to $Ca^{2+}$ sites, and Arabic numbers to the positions of selected residues. After drawing by Jane S. Richardson.

The aim of the present work has been to produce a detailed picture of the $Ca^{2+}$-induced effects on dynamics and structure through measurements of the exchange rates for as many as possible of the 71 backbone amide hydrogens in calbindin $D_{9k}$, in both the $Ca_2$ and apo forms. Quenching of amide proton exchange by rapidly lowering the pH to around 3 has previously been used to detect intermediates on protein folding pathways (Kuwajima et al., 1983; Udgaonkar & Baldwin, 1988; Roder et al., 1988). Here an experiment in which the $Ca^{2+}$ ion itself is used as a quencher is introduced. The large retardation of hydrogen exchange as a result of $Ca^{2+}$ binding is used to achieve the necessary time resolution to obtain exchange rates in the apo state.

There is no theory that quantitatively accounts for amide proton exchange rates in proteins. These rates are, however, often thought to be correlated with structural elements such as hydrogen bonding and solvent accessibility. These properties can be roughly evaluated from the crystal conformation, but some of the solvent effects can be included by molecular dynamics simulation starting from the crystal conformation but providing an aqueous environment. We report on the evaluation of hydrogen bonding and solvent accessibility of amide hydrogens from two such simulations of calcium-loaded calbindin $D_{9k}$. One simulation was based on a model using atoms (Ahlström et al., 1989), and the other used explicit hydrogen atoms throughout (Teleman et al., unpublished experiment). The hydrogen bonding and solvent accessibility in the simulations and in the crystal conformation are discussed with respect to measured exchange rates.

## Experimental Procedures

*Materials.* Bovine calbindin $D_{9k}$ was expressed in *Escherichia coli* (Brodin et al., 1986, 1989) and purified as previously described (Johansson et al., 1990). Apo protein was prepared as described (Linse et al., 1987), and the residual $Ca^{2+}$ content was below 0.05 mol of $Ca^{2+}$/mol of calbindin, as judged from 1D $^1H$ NMR spectra and $Ca^{2+}$ titrations in the presence of the $Ca^{2+}$ chelator quin 2. $^1H$ NMR spectra were obtained at 500.13 MHz on a GE OMEGA 500 spectrometer, with protein concentration in the range 1–4 mM. All exchange rates were measured at pH 7.5, room temperature, and low ionic strength (no added salt). No corrections were made for isotope effects on pH values.

*Slow NH Exchange in the $Ca_2$ Form.* The slowly exchanging NH's in the $Ca_2$ form were studied in a direct exchange-out experiment in which the protein (in $H_2O$) was 15-fold diluted with $D_2O$ at time zero. One-dimensional $^1H$ NMR spectra were recorded at 14 different exchange times, $t$, ranging from 12 min to 6 months. Each spectrum was recorded for a time ranging from 2 min (first spectrum) to 32 min (all spectra started more than 43 min after dilution with $D_2O$), and $t$ was taken as the average exchange time of the spectrum. An identical exchange-out experiment was performed, but this time 90-min two-dimensional (COSY) spectra were started at 33, 135, and 380 min after dilution with $D_2O$. The exchange rates for individual amide protons were determined from least-squares fitting to the intensities, $I$, of the corresponding NH resonances or NH–$C_\alpha$H cross-peaks [measured in cross sections parallel to the $\omega_2$ axis at $\omega_1$ of the $C_\alpha$ proton; see Qiwen et al. (1987)] as a function of $t$. For resolved NH resonances and cross-peaks, a functional form of

$$I = C + A \exp(-kt)$$

was used, and

$$I = C + A_1 \exp(-k_1 t) + A_2 \exp(-k_2 t)$$

for pairs of overlapping resonances.

*NH Exchange in the Apo Form.* The exchange in the apo form is much faster than in the $Ca_2$ form and was studied in a quenching experiment. Apo calbindin in $H_2O$ (pH 7.5) was 15-fold diluted with $D_2O$ (pH 7.5) at time zero. At a time $\tau$ later, the exchange in the apo state was quenched by addition of saturating amounts of calcium and adjustment of the pH to 6.0, followed by acquisition of 1D or 2D (COSY) $^1H$ NMR spectra. The actual values of the exchange times $\tau$ were 0, 10, 20, 42, 90, 300, 600, 1200, 2400, and 7200 s in the 1D case and 10 and 90 s in the 2D case. The exchange rates for individual amide protons were determined as described above for the exchange-out experiment but now as a function of $\tau$.

*Fast NH Exchange in the $Ca_2$ Form.* Amide protons whose exchange in the $Ca^{2+}$ form was complete within ca. 10 min could not be studied for either of the two forms with the exchange-out and quenching techniques. For these protons the exchange rates in the $Ca_2$ form were determined by the 1D or 2D $^1H$ NMR saturation transfer method (Pitner et al., 1974). This method is based on the fact that when water protons substitute for amide protons, the water protons will carry their saturation into their new existence as amide protons. Saturation transfer can be used successfully for amide protons with half-lives in the range $0.1T_1$ to $10T_1$, where $T_1$ is the longitudinal relaxation time of the amide proton. From measurements of $T_1$ (or $T^*_1$; cf. below) and the intensities ($I$) of a specific $^1H$ NMR resonance in two or more experiments with presaturation of the water resonance for different times, it is possible to calculate the exchange rate for the corresponding amide proton (Forsén & Hoffman, 1963) with the equation

$$I(t_{presat}) = I(0)(1 + kT^*_1[\exp(-t_{presat}/T^*_1) - 1])$$

where

$$1/T^*_1 = 1/T_1 + k$$

and $k$ is the exchange rate constant (Forsén & Hoffman, 1963). For each resolved resonance, $T^*_1$ was obtained directly from a single-exponential fit to a standard inversion–recovery experiment with saturation of the water signal. For resolved resonances intensities were measured in 1D $^1H$ NMR in a one-pulse experiment with $t_{presat} = 3.0$ s and a jump-and-return experiment ($t_{presat} = 0$) (Plateau & Guéron, 1982). The latter pulse sequence creates shift-dependent excitation, but this was not a problem here, as in all cases nearby (within 0.2 ppm) resonances from slowly exchanging hydrogens provide internal standards for the intensities. After calculation of the exchange

rates, an average value of $T_1$ of 1.0 s could be obtained and was used in subsequent calculations for resonances overlapping in 1D NMR as deviations from average were small. For these resonances, intensities were measured in two 2D $^1$H NMR COSY experiments with $t_{presat}$ = 0.25 s (and a 1.75-s delay) and $t_{presat}$ = 2.0 s.

The $^1$H NMR spectrum of $Ca_2$ calbindin has been fully assigned at pH 6.0 (Kördel et al., 1989). The assignments at pH 7.5 were close to those at pH 6.0 and were obtained from a series of relayed COSY spectra in the pH range 6.0–7.5.

*Hydrogen Bonding and Solvent Accessibility.* Two molecular dynamics simulations of calbindin were performed according to standard techniques as implemented in the simulation program MUMOD (Teleman & Jönsson, 1986). Both simulations lasted 160 ps (of which 40 ps was considered as equilibration). The one using united atoms has been fully described elsewhere (Ahlström et al., 1989), and a full description of the one with all atoms explicitly described will be given (Teleman et al., unpublished experiment).

Hydrogen bonds were evaluated with an asymmetric criterion such that a hydrogen bond is considered to be formed when the hydrogen–acceptor distance becomes less than 2.4 Å and the donor–hydrogen–acceptor angle at the same time exceeds 135°. The bond is deemed to cease when either the distance exceeds 3.0 Å or the angle becomes less than 90°. The reason for the asymmetry is that unfavorable encounters may not result in a hydrogen bond, while, on the other hand, a bond already formed may vibrate and occasionally be very long without actually breaking.

The solvent accessibility was evaluated as follows. The amide proton and a water molecule were taken to be in contact at a distance of 2.4 Å. This is somewhat farther away than the expected length of a hydrogen bond, but smaller than the sum of amide proton and water van der Waals radii. Two atoms were considered not to interfere if their Lennard–Jones interaction was negative; i.e., their separation was larger than $2^{-1/6} = 0.891$ times the sum of their van der Waals radii. The water van der Waals radius was taken to be 1.78 Å. The accessibility was then determined as the area on a contact sphere of radius 2.4 Å around each amide proton where a water molecule would not interfere with any other protein atom. This area is trivial to calculate if at most one neighbor interferes, but otherwise, the algebra is difficult because the blocked regions may overlap. This difficulty was circumvented by randomly sampling the contact sphere and discarding sampling points blocked by neighbors. For each case 10000 samples were used, providing an accuracy of 1%. The surface area of a horizontal slice of thickness d$z$ is independent of the position $z$. Hence, a simple way to obtain an even distribution of random points on a sphere is to use rectangular random distributions in $z \in [-R, R]$ and the azimuthal angle $\varphi \in [-\pi, \pi]$, where $R$ is the sphere radius. The accessibility was evaluated every 4.8 ps, i.e., 27 times, and the average is presented.

## Results and Discussion

Through the combined use of various NMR techniques, it has been possible to determine a full set of amide proton exchange rates in $Ca_2$ calbindin at pH 7.5 and 25 °C. The time dependence of the intensities of well-resolved $^1$H NMR resonances (Figure 2a) or NH–$C_\alpha$H cross-peaks in 2D COSY spectra (Figure 3) was used to calculate exchange rates for slowly exchanging protons ($k \leq 10^{-2}$ s$^{-1}$ and $k \leq 10^{-3}$ s$^{-1}$, respectively). Higher rates ($k$ = 0.1–6 s$^{-1}$) were determined from saturation-transfer experiments in 1D (Figure 4) and 2D (COSY) NMR. For one proton (Leu28) it was possible to determine an upper limit ($k < 6 \times 10^{-9}$ s$^{-1}$) only, and for three protons (Lys1, Gly18, and Leu46) only a lower limit ($k > 6$ s$^{-1}$) was obtained, but this limit is close to the exchange rates of free peptide NH's at pH 7.5 and 25 °C (cf. below). The NH exchange in apo calbindin was studied in a quenching experiment, which could be used for protons that have exchange rates lower than ≈0.01 s$^{-1}$ in the $Ca_2$ form. Thus, 38 out of 71 amide proton could be studied in the apo form and were used in analysis of the effects of calcium binding on structure and dynamics of the protein. The final results are presented in Table I and Figure 5. The exchange rates for fully solvent-exposed peptide chain (intrinsic exchange rates) were calculated with the data of Molday et al. (1972) to take into account the effects of the neighboring amino acid side chains. The average intrinsic rate constant for calbindin at pH 7.5 and 25 °C is 46 s$^{-1}$, and the values for individual NH's span from 21 to 210 s$^{-1}$. We have chosen to use the average value as a base line in Figure 5. The height of each bar than represents an estimate of the retardation of NH exchange imposed by the protein structure.

*$Ca_2$ Form.* The $Ca^{2+}$-loaded form of calbindin appears to be a very compact and rigid protein since a number of amide protons are highly protected against exchange with solvent molecules. At pH 7.5 and 25 °C the exchange of as much as 30 of the 71 backbone amide protons is retarded more than 5 orders of magnitude as compared to that of fully solvent-exposed polypeptide strand. Slowly exchanging amide hydrogens have been found primarily in β-sheet structures and S–S bridged proteins (Wüthrich et al., 1984), for example, BPTI. The structure of calbindin $D_{9k}$ is however dominated by four α-helices connected by loops, the first and third of which wrap around the $Ca^{2+}$ ions to supply the $Ca^{2+}$ ligands. A short β-sheet is formed between the two $Ca^{2+}$-binding loops, and the protein has no cysteine residues. The slow NH exchange is in line with the high stability of $Ca_2$ calbindin, which does not denature either in 8 M urea or at 100 °C (Wendt et al., 1988).

*Secondary Structure.* The sequential pattern of NH exchange rates in $Ca_2$ calbindin can be correlated with the position of secondary structure elements as observed in the crystal structure (Szebenyi & Moffat, 1986) and solution (Kördel et al., 1989). Figure 5 clearly shows that the C-terminal half of calbindin is considerably more flexible than the N-terminal half, with the second helix constituting an exceptionally stable part of the protein. Leu28 is extreme—no intensity changes could be detected for its NH resonance in the exchange-out experiment, even at 6 months after dilution with $D_2O$. In the N-terminal half there is a strong correlation between low exchange rate and location in an α-helix, while in the C-terminal half this correlation does not exist. Residues 41–49 seem to constitute the most flexible part of calbindin. It has previously been shown that the peptide bond between Gly42 and Pro43 undergoes cis–trans isomerization with interconversion rates of 0.2 and 0.07 s$^{-1}$ for cis → trans and trans → cis, respectively, at room temperature (Kördel et al., 1990; Chazin et al., 1989). It thus seems likely that location within a flexible segment of the protein allows this peptide bond to isomerize to an observable extent also in the folded state.

*Solvent Accessibility and Hydrogen Bonding.* The solvent-accessible surface area for a given protein atom is defined as the area over which the center of a water molecule can be placed while retaining contact with that atom but not penetrating any other atom. In calbindin the accessible surface area is zero for most amide protons, both in the crystal structure and in solution as modeled by the all-atoms simu-

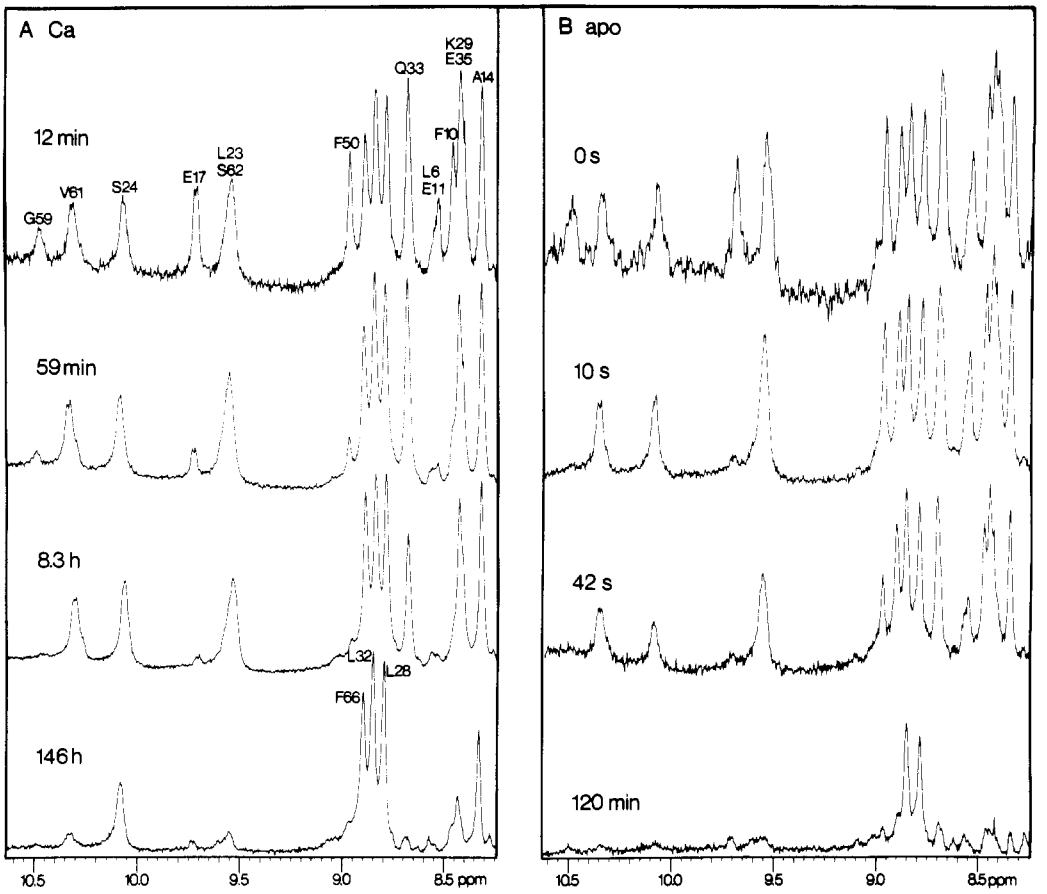


FIGURE 2: (A) Exchange-out experiment on $Ca_2$ calbindin and (B) quenching experiment on apo calbindin. Selected region of representative spectra is shown. Resources are identified in (A). Time after dilution with $D_2O$, $t$, is indicated in (A), and the exchange time in the apo form, $\tau$, is indicated in (B) (see Experimental Procedures). Note that for the top spectrum in (A) only a few transients were recorded in order to get an early spectrum.

lation (cf. Figure 5). The correlation between crystal and simulation results is strong, but for most protons the solvent accessibility is larger in the simulation than in the crystal form. This is due to fluctuations allowed for in the simulation and probably represents a more realistic picture of accessibility than available from the static crystal structure. However, the time scale of motions captured in a 120-ps simulation are many orders of magnitude less than the time scale of exchange reactions. Therefore, the dynamic accessibility determined from the simulations may not pertain to the dynamic accessibility assayed in hydrogen exchange. Hydrogen bonds in the crystal were identified with the following criteria (Szebenyi & Moffat, 1986): donor–acceptor distance, ≤3.2 Å; N–H–X angle, 145–180° (filled symbols in Figure 5). For possible hydrogen bonds, values of ≤3.6 Å and 110–180°, respectively, were used. In the present simulations hydrogen bonds are generated by Coulombic interactions, and no separate potential has been devised to provide hydrogen bonds. The drawback of this approach is that the polarization occurring in a hydrogen bond is neglected. Instead of a 10–20 kJ/mol potential well at an acceptor–hydrogen distance of 1.8–2.0 Å, which characterizes a physical hydrogen bond, the minimum is, in the present case, more shallow and farther away (cf. Figure 6). Analysis of hydrogen bonds amounts to counting the population in the bonding potential well. From Figure 6, this would include anything up to an acceptor–hydrogen distance of about 3.5 Å, or at least 1 Å longer than that generally considered as a hydrogen bond. Instead, we have chosen to apply a hydrogen-bond criterion appropriate for a physical hydrogen bond (see Experimental Procedures). Under this criterion even several of the α-helix-stabilizing hydrogen bonds seem weak, but with a criterion based on Figure 6 the hydrogen-bond network is very stable indeed (data not shown). The general picture is nevertheless independent of criterion, although with differences in occupation frequency. Quantum mechanical calculations on the uracil–water interaction are in progress (Gunnar Karlström and per-olof Åstrand, personal communication) to provide a better potential for hydrogen bonds.

*Correlation of Solvent Accessibility and Hydrogen Bonds with Exchange Rates in $Ca_2$ Calbindin.* The hydrogen-bonding networks and solvent accessibilities in the crystal structure and in the two simulations are displayed in Figure 5. In the N-terminal half of calbindin the accessibilities and hydrogen-bonding networks are highly similar in the crystal and in both simulations, and the correlation with measured exchange rates is strong. The exchange rate is fast for solvent-accessible protons, i.e., for Lys1, Ser2, Glu4, Gly18, Asp19, and Lys25. Only for Asn21 and Gln22 is there a notable difference between simulation and crystal. In the crystal structure the NH of Asn21 seems strongly hydrogen bonded, whereas the Gln22 NH is not, and none of them is solvent accessible. In contrast, the Asn21 NH exchanges relatively quickly ($k \approx 0.3\ s^{-1}$) and the Gln22 NH slowly ($k = 6 \times 10^{-6}\ s^{-1}$). Both simulations, however, indicate that Asn21 is slightly accessible to water, and a hydrogen bond involving Gln22 NH is roughly twice as frequently populated as that of Asn21 NH. We thus conclude that the solution and crystal structures of the N-terminal half of calbindin are nearly identical, except for a subtle conformational difference involving Asn21 and Gln22 in the $Ca^{2+}$-binding loop. In the C-terminal half, on the other hand, the crystal and simulations

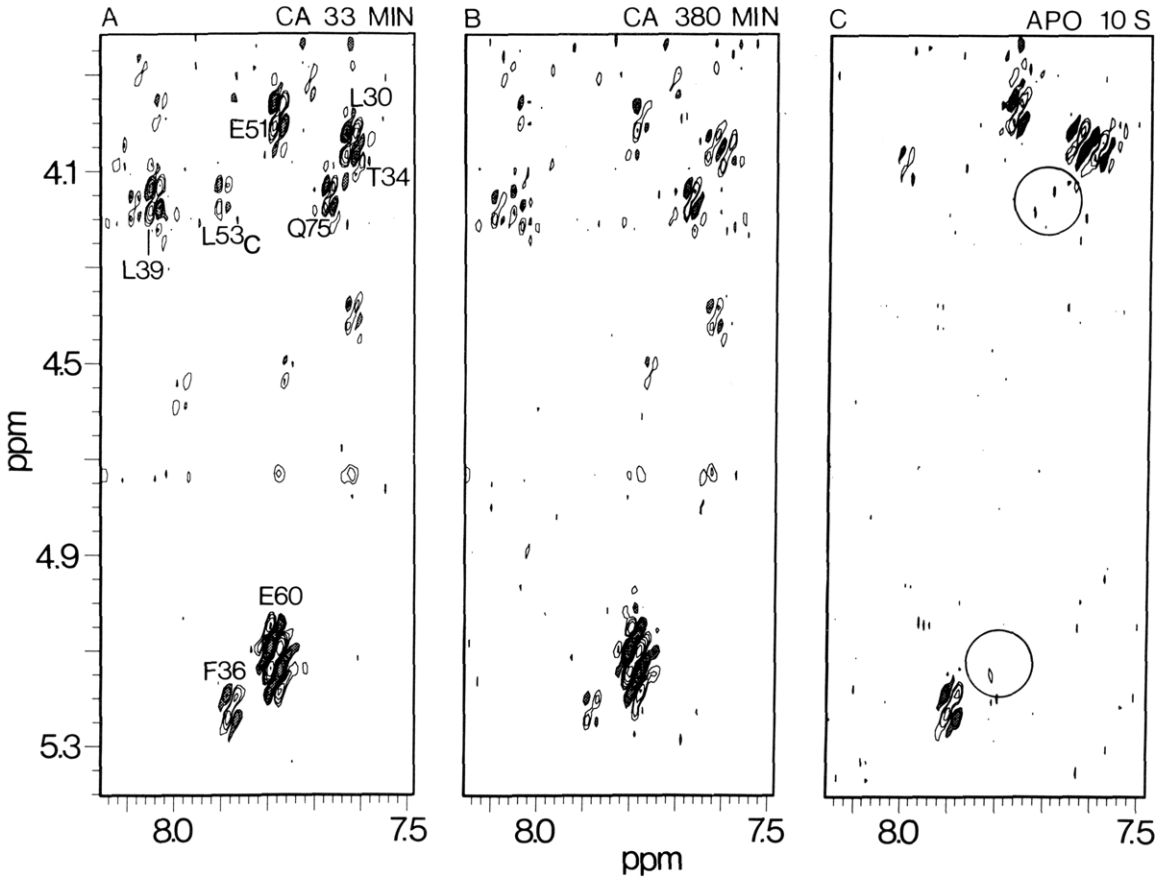


FIGURE 3: Selected region of 2D COSY spectra (recorded during 90 min on 1 mM protein solution) for the exchange-out experiment (A and B) (exchange time, $t$, at start indicated) and the quenching experiment (C) (exchange time in the apo form, $\tau$, indicated).

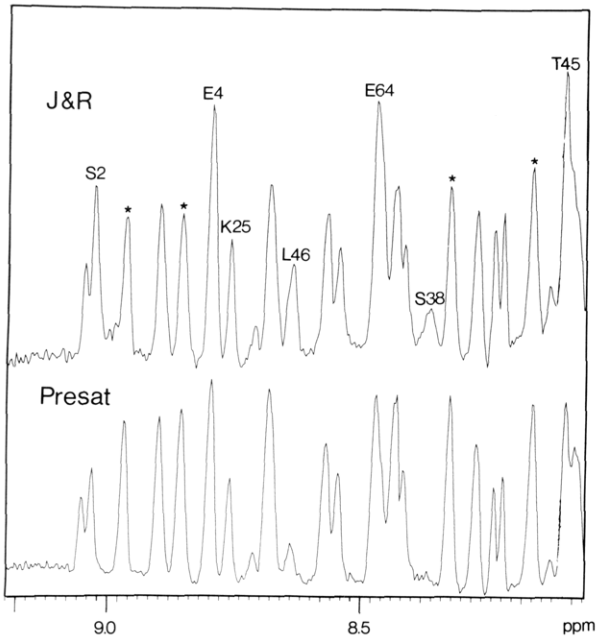


FIGURE 4: Transfer of solvent saturation experiment. (Top) Spectrum recorded with the jump and return pulse sequence, which suppresses the water resonance without affecting the magnetization of the water protons. (Bottom) Spectrum recorded after presaturation of the water resonance for 3 s. These spectra have been resolution enhanced. The resonance marked L46 in the J&R spectrum overlaps with T45 in the *cis*-Pro43 form of the protein, and the remaining intensity in the presat spectrum comes from $T45_{cis}$ only, as judged from 2D NMR spectra.

provide three different pictures of hydrogen bonds and solvent accessibilities. Both the simulations and the crystal structure can explain the fast exchange rates measured for Ser38, Leu46, Asn56, and Phe63. We will focus on two regions where the three studied cases provide different pictures, Asp58 through Glu60 and Gln75. The region involving Lys41 through Leu49 will not be discussed here since the simulations only sample the *trans*-Pro43 conformation and the crystal structure most likely represents an intermediate between the cis and trans conformations.

The Gln75 NH is found to exchange slowly. In the crystal structure this NH is involved in a weak hydrogen bond, and the accessibility is zero, whereas it is accessible in both simulations and the hydrogen-bonding frequency is 10% or less. This residue, which is at the C-terminus, is highly mobile in the crystal structure (Szebenyi & Moffat, 1989) and possibly also in solution since no NOE has been detected for its NH (Kördel et al., 1989). The NH exchange data thus suggest that the end of the fourth helix moves as a packet and that the hydrogen bond involving Gln75 NH is not broken by this motion. The backbone amide protons of Gly58 through Gln60 are found to exchange slowly. In the all-atoms simulation they are accessible and appear not to be hydrogen bonded, but in the united-atoms MD simulation they are not accessible and seem to be hydrogen bonded. In the united-atoms simulation the side chain of Glu60 moves substantially from its position in the initial configuration, the crystal structure, and its carboxylate side chain actually becomes a ligand to the $Ca^{2+}$ ion in site I. In the all-atoms simulation the Glu60 side chain moves in the other direction but continues to fluctuate back and forth. Mutational studies show that shortening of the side chain (Glu60 → Asp) dramatically reduces the $Ca^{2+}$ affinity of calbindin, $\Delta p(K_1K_2) = 1,2$, whereas removal of the charge on the side chain (Glu60 → Gln) results in a very modest decrease, $\Delta p(K_1K_2) = 0.2$ (Linse et al., unpublished results). These results cannot be explained by electrostatic effects but

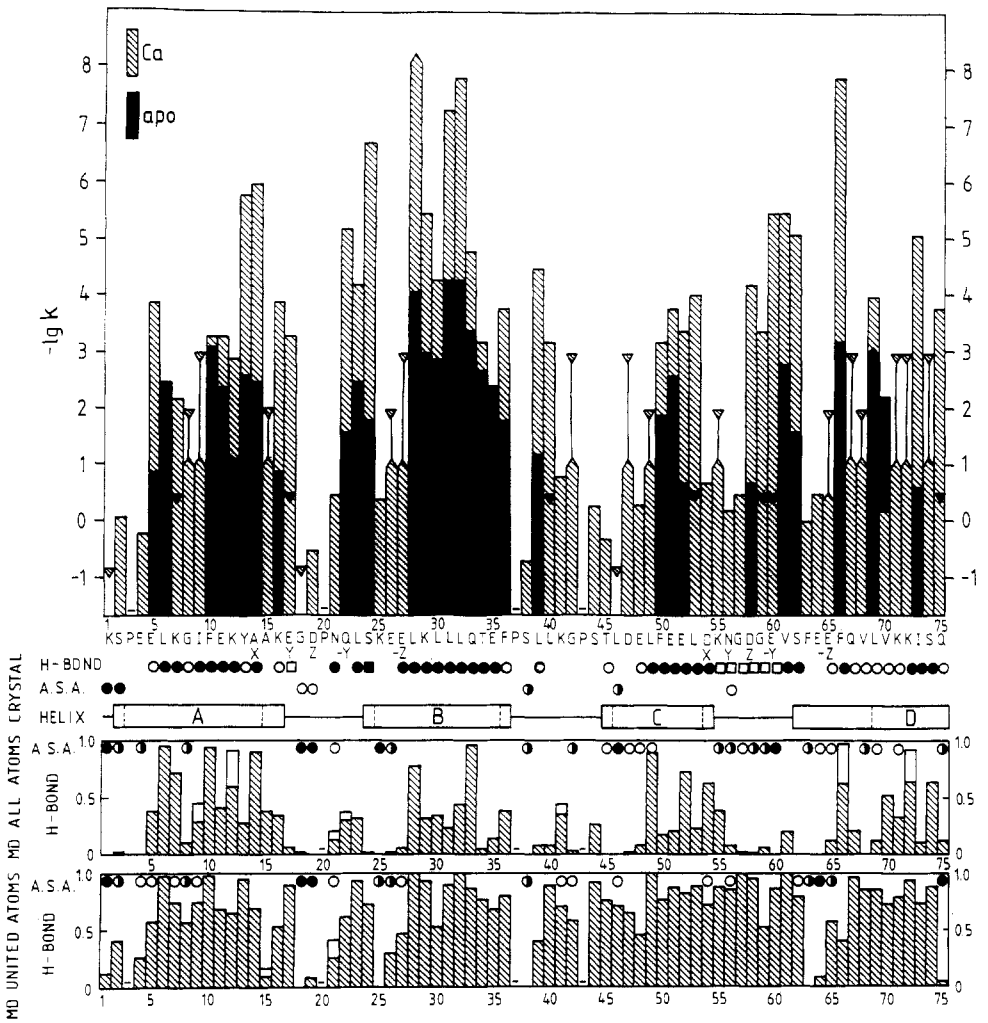


FIGURE 5: (Top) Exchange rates for individual backbone amide protons in apo and $Ca^{2+}$-loaded calbindin $D_{9k}$ at pH 7.5 and 25 °C. The NH proton of each residue is represented by a vertical bar with the top of the shaded part indicating $-\log k$ ($k$ in $s^{-1}$) in the $Ca^{2+}$ form and with the top of the black part of the bar corresponding to $-\log k$ in the apo form. The base line is drawn at $\log k = 1.66$, which is the average of the exchange rates in freely exposed chain for all 75 NH protons at pH 7.5, 25 °C, Molday (1972) factors being used to compensate for primary-structure effects. Shaded and filled triangles represent upper limits for $-\log k$ in the $Ca^{2+}$ and apo forms, respectively. Pointed bars represent lower limits. (Bottom) Solvent-accessible surface areas (A.S.A.) and hydrogen bonds are displayed as follows. *For the Crystal Structure*: H-bonds [from Szebenyi and Moffat (1986)], (●) donor–acceptor distance of ≤3.2 Å and N–H–X angle of 145–180° and (○) "possible hydrogen bond" with limits of ≤3.6 Å and 110–180°, respectively (square symbols are used for hydrogen bonds between NH's and calcium-coordinating oxygens); A.S.A., (●) more than 5% of the contact sphere (of 72.4 Å$^2$), (◑) 1–5%, and (○) 0.1–1%. *For each simulation*: Shaded bars show the fraction of the simulated time that each NH is H-bonded due to the criterion described under Experimental Procedures. For some hydrogen bonds the occupancy is somewhat uncertain and lies in the interval indicated by the tops of the shaded and white bars. Symbols for A.S.A.: (●) more than 5% of the contact sphere (of 72.4 Å$^2$); (◑) 1–5%; (○) 0.1–1% (draw in the upper part of the H-bond diagram).

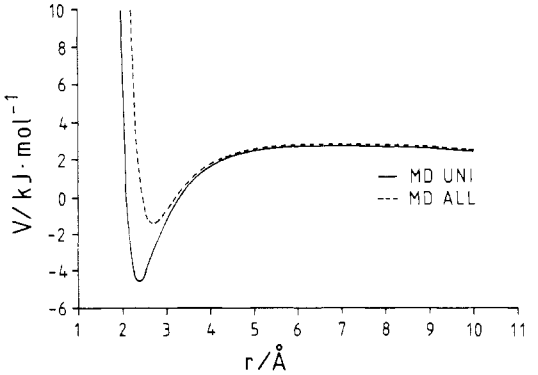


FIGURE 6: Potential energy for the interaction of an NH group with a carbonyl oxygen as modeled by the Coulomb and Lennard–Jones terms in the force field. No explicit hydrogen-bond potential is used. (—) United-atoms force field; (– –) all-atoms force field.

may be due to some structural role of the side chain. As a ligand in site I it may easily have such a role, but not if fluctuating as in the all-atoms simulation. The all-atoms simulation was found to produce more realistic results than the united-atoms simulation as regards overall dynamics, local dynamics of Tyr13, and quadrupolar relaxation of the calcium ions. From the mutation studies, however, it appears that the local structure of Glu60 is better described in the united-atoms simulation. On the basis of the exchange data, the structure of the C-terminal half of calbindin can be concluded to differ between crystal and solution at several points. The starting configuration for the simulations is thus not as close to the solution structure as for the N-terminal half, which may explain why none of the simulations can explain all NH exchange rates within the C-terminal half.

*Effects of $Ca^{2+}$ Binding.* The comparison of the apo and $Ca_2$ calbindins will be limited to 38 amide hydrogens with slow exchange in the $Ca_2$ form. The overall picture is that removal of $Ca^{2+}$ produces an average increase in these rates by a factor of 220. This is a large difference in light of previously determined effects of ligand binding in other types of proteins (Lennick et al., 1981) but in good correlation with the observed differences in stability between $Ca_2$ and apo calbindin. The

Table I: Amide Proton Exchange Rates (log $k$, with $k$ in $s^{-1}$) in Calbindin at pH 7.5 and 25 °C at Low Ionic Strength

| | $Ca_2$ calbindin | | apo calbindin | | | $Ca_2$ calbindin | | apo calbindin | |
|---|---|---|---|---|---|---|---|---|---|
| residue | log $k$ | method[a] | log $k$ | method | residue | log $k$ | method[a] | log $k$ | method |
| Lys1 | ≥0.8 | ST | *b* | | Leu39 | −4.5 | 1EXP | −1.2 | 1EXQ |
| Ser2 | −0.1 | ST | *b* | | Leu40 | −3.2 | 2D | ≥−0.5 | 2DQ |
| (Pro3) | | | | | Lys41 | −0.8 | ST2D | *b* | |
| Glu4 | 0.2 | ST | *b* | | Gly42 | −2.0 ± 1.0 | 2D,ST2D | *b* | |
| Glu5 | −3.9 | 1EXP | −0.9 | 1EXQ | (Pro43) | | | | |
| Leu6 | −2.3 ± 0.3 | 1EXP | −2.5 | 1EXQ | Ser44 | −0.3 | ST | *b* | |
| Lys7 | −2.2 | 1EXP | ≥−0.5 | 1EXQ | Thr45 | 0.3 | ST2D | *b* | |
| Gly8 | −1.5 ± 0.5 | 2EXP,ST | *b* | | Leu46 | ≥0.8 | ST | *b* | |
| Ile9 | −2.0 ± 1.0 | 2D,ST | *b* | | Asp47 | −2.0 ± 1.0 | 2D,ST2D | *b* | |
| Phe10 | −3.3 | 1EXP | −3.1 | 1EXQ | Glu48 | −0.3 | ST2D | *b* | |
| Glu11 | −3.3 | 1EXP | −2.4 | 1EXQ | Leu49 | −1.5 ± 0.5 | 2EXP,ST | *b* | |
| Lys12 | −2.9 | 1EXP | −1.1 | 1EXQ | Phe50 | −3.2 | 1EXP | −1.9 | 1EXQ |
| Tyr13 | −5.8 | 1EXP | −2.6 | 1EXQ | Glu51 | −3.8 | 2EXP,2D | −2.6 | 2EXQ,2DQ |
| Ala14 | −6.0 | 1EXP | −2.5 | 1EXQ | Glu52 | −3.4 | 2D | −0.7 | 1EXQ |
| Ala15 | −1.5 ± 0.5 | 1EXP,ST | *b* | | Leu53 | −4.0 | 2D | ≥−0.5 | 2DQ |
| Lys16 | −3.9 | 2D | −0.9 | 2DQ | Asp54 | −0.7 | ST2D | *b* | |
| Glu17 | −3.3 | 1EXP | ≥−0.5 | 1EXQ | Lys55 | −1.5 ± 0.5 | 1EXP,ST | *b* | |
| Gly18 | ≥0.8 | ST | *b* | | Asn56 | −0.2 | ST2D | *b* | |
| Asp19 | −0.5 | ST | *b* | | Gly57 | −0.5 | ST2D | *b* | |
| (Pro20) | | | | | Asp58 | −4.2 | 1EXP | −0.7 | 1EXQ |
| Asn21 | −0.5 ± 0.2 | ST,ST2D | *b* | | Gly59 | −3.4 | 1EXP | ≥−0.5 | 1EXQ |
| Gln22 | −5.2 | 1EXP | −1.6 | 1EXQ | Glu60 | −5.5 | 2EXP,2D | ≥−0.5 | 2EXQ,2DQ |
| Leu23 | −4.2 | 2EXP,2D | −2.5 | 2EXQ,2DQ | Val61 | −5.5 | 1EXP | −2.8 | 1EXQ |
| Ser24 | −6.7 | 1EXP | −1.8 | 1EXQ | Ser62 | −5.1 | 2EXP,2D | −1.6 | 2EXQ,2DQ |
| Lys25 | −0.4 | ST | *b* | | Phe63 | 0.0 | ST | *b* | |
| Glu26 | −1.5 ± 0.5 | 2EXP,ST | *b* | | Glu64 | −0.5 | ST | *b* | |
| Glu27 | −2.0 ± 1.0 | 2D,ST2D | *b* | | Glu65 | −0.3 | ST2D | *b* | |
| Leu28 | <−8.2 | 1EXP | −4.1 | 1EXQ | Phe66 | −7.9 | 1EXP | −3.2 | 1EXQ |
| Lys29 | −5.5 | 1EXP | −3.0 | 1EXQ | Gln67 | −2.0 ± 1.0 | ST2D,2D | *b* | |
| Leu30 | −4.3 | 2D | −2.9 | 1EXQ | Val68 | −1.5 ± 0.5 | 1EXP,ST | *b* | |
| Leu31 | −7.3 | 1EXP | −4.3 | 1EXQ | Leu69 | −4.0 | 2D | ≤−3.0 | 2DQ |
| Leu32 | −7.9 | 1EXP | −4.3 | 1EXQ | Val70 | −0.2 | ST | −2.2 | 2DQ |
| Gln33 | −4.8 | 1EXP | −3.4 | 1EXQ | Lys71 | −2.0 ± 1.0 | 2D,ST2D | *b* | |
| Thr34 | −3.2 | 1EXP | −2.7 | 1EXQ | Lys72 | −2.0 ± 1.0 | 2D,ST2D | *b* | |
| Glu35 | −2.0 ± 0.3 | 1EXP | −2.4 | 1EXQ | Ile73 | −5.1 | 2D | −0.6 | 2DQ |
| Phe36 | −3.8 | 1EXP | −1.8 | 1EXQ | Ser74 | −2.0 ± 1.0 | 2D,ST2D | *b* | |
| (Pro37) | | | | | Gln75 | −3.8 | 2D | ≥−0.5 | 2DQ |
| Ser38 | 0.7 | ST | *b* | | | | | | |

[a] The results for the $Ca_2$ form were obtained from one- (1EXP) or two- (2EXP) exponential fitting to exchange-out data by 1D $^1H$ NMR, to exchange-out data by 2D $^1H$ NMR (2D), or to solvent saturation transfer data by 1D (ST) or 2D (ST2D) $^1H$ NMR. The results for the apo form were obtained from one- (1EXQ) or two- (2EXQ) exponential fitting to data from quenching experiments by 1D or 2D $^1H$ NMR (2DQ). [b] Not determined.

latter is, at pH 7.5, half denatured either at 84 °C or in 5.2 M urea (25 °C), whereas the former foes not denature either in 8 M urea or at 100 °C (Wendt et al., 1988). Looking at Figure 5 we note that the NH exchange in the $Ca_2$ form is spread over ca. 10 orders of magnitude and there are in many cases large differences for amide protons of neighboring residues. The exchange in this form thus appears to be governed primarily by local fluctuations involving one to three residues. The fact that Leu28 does not exchange to any observable extent during 0.5 year also indicates that the event of global opening is very rare. In the apo state, on the other hand, a large portion of the low rates lie in the range $10^{-4}$–$10^{-2}$ $s^{-1}$, and many sequential neighbors show similar rates. It is therefore plausible that in the apo form the exchange of the most protected NH's is the result of a common opening process. A better understanding of the backbone dynamics involved could come from studies of the temperature and pH dependence of NH exchange rates in both forms. It we focus on helix B, where there is a continuous stretch of nine residues for which information could be obtained for both forms, we first note that this helix appears to be intact after $Ca^{2+}$ removal. In the $Ca^{2+}$ form there are large differences in exchange rates of NH's within the helix. In the crystal structure, NH's of Leu28, Leu31, and Leu32 are all on the inside of the helix and exchange extremely slowly, whereas NH's of Lys29, Leu30, Gln33, and Thr34 are on the solvent-exposed side and exchange several orders of magnitude faster (but still slowly). In the apo form the differences between the two sides of the helix are much smaller.

*Effects on the β-Sheet.* A careful analysis of individual residues may yield detailed information on the effects of calcium binding on the calbindin molecule. First, we focus on the short antiparallel β-sheet between the two $Ca^{2+}$ sites. Two hydrogen bonds connect one residue in each strand—Leu23 C=O to Val61 NH and Leu23 NH to Val61 C=O. It has been inferred from the pattern of cross-strand NOE's that this β-sheet is not broken when calbindin releases $Ca^{2+}$ (Skelton et al., 1989). The present data support this finding; the exchange rates for the NH's of Leu23 and Val61 are slow also in the apo form (log $k$ = −2.8 and −2.5, respectively). Similar mini-β sheets have been observed within pairs of EF-hands in several proteins in the calmodulin family (Kretsinger, 1987), but the effect of $Ca^{2+}$ removal differs. In the case of the C-terminal tryptic fragment of calmodulin (containing sites III and IV), the β-sheet appears to be formed in both the presence and absence of $Ca^{2+}$ (Ikura et al., 1985), whereas in the C-terminal domain of troponin C calcium appears to be a prerequisite for β-sheet formation (Tsuda et al., 1988).

*Effects on $Ca^{2+}$ Binding Loops.* In Table II we list all residues for which the amide proton exchange rates increase more than 3 orders of magnitude upon removal of $Ca^{2+}$. Large

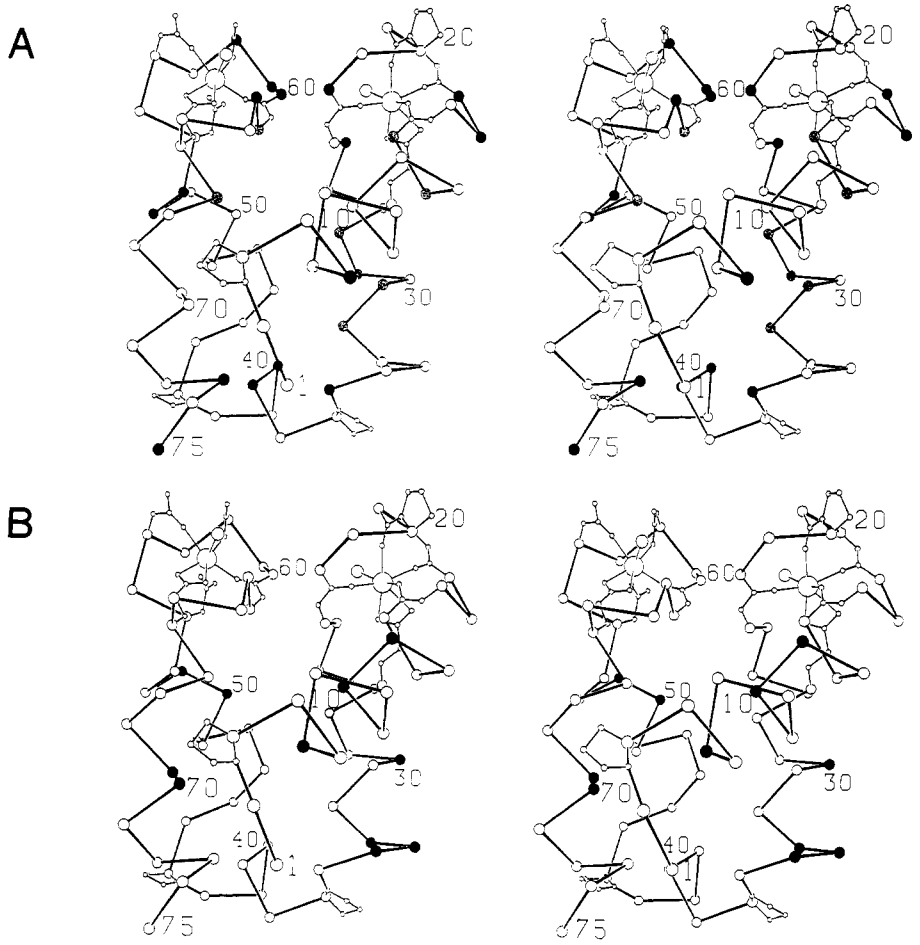


FIGURE 7: Stereoview of the α-carbon skeleton of bovine calbindin $D_{9k}$ in the crystal state. $Ca^{2+}$ ligands are explicity shown. (A) α-Carbons of residues with a large increase in NH proton exchange rate as a consequence of $Ca^{2+}$ removal ($\log k_{apo} - \log k_{Ca} \geq 2$) are marked. Black α-carbons mean that $\log k_{apo} \geq -2$ and gray that $\log k_{apo} < -2$. (B) Black α-carbons are used for residues with small effects on NH exchange rates ($\log k_{apo} - \log k_{Ca} < 1.4$). For all these, $\log k_{apo} < -2$. Stereopicture kindly provided by Doletha M. E. Szebenyi, Cornell University.

effects of $Ca^{2+}$ removal are seen in the loop regions for a few amide protons which in the $Ca_2$ form are hydrogen bonded to $Ca^{2+}$-liganding oxygens—carboxyl or carbonyl (cf. Figure 5 in which squares in the H-bond lists indicate this type of interaction). Five out of the twelve amide protons that are most affected by calcium release belong to this category. For Ser24 and Glu60, removal of $Ca^{2+}$ increases the NH exchange rates by a factor of $10^5$ or more. Structural rearrangements in the $Ca^{2+}$-binding loops are indicated by the fact that the NH exchange of Lys16, Glu17, Asp58, Gly59, and Glu60 changes from slow ($k < 5 \times 10^{-4}$) to fast ($k > 0.1\ s^{-1}$) when $Ca^{2+}$ is removed from calbindin. The hydrogen bonds of these NH's may thus be broken or weakened in the apo state. Gly59 is located between $Ca^{2+}$ ligands at octahedral positions $z$ (Asp58) and $-y$ (Glu60) in site II. It has been noted that a glycine in this position is a highly conserved feature of EF-hand $Ca^{2+}$-binding sites (Kretsinger, 1980). The amide protons of the corresponding glycines in the four $Ca^{2+}$ sites of calmodulin (Ikura et al., 1987) and in the two $Ca^{2+}$ sites in the C-terminal domain of troponin C (Tsuda et al., 1988) have, on the basis of the $Ca^{2+}$ dependence of $^1H$ NMR chemical shifts, been shown to participate in hydrogen bonds that are weakened or broken in the absence of $Ca^{2+}$. This particular $Ca^{2+}$-induced effect could then be expected to occur in most EF-hand proteins, and the $Ca^{2+}$-dependent hydrogen bonds involving the conserved glycines are likely to play a role in the biological functions of these proteins.

*Distant Effects.* Surprisingly, large effects are seen for Glu5, Ile73, and Gln75, the amide protons of which are located more than 17 Å away from the $Ca^{2+}$ ions in the crystal structure. Hydrogen bonds involving the NH's of Glu5 and Gln75 are the first H-bond in helix A and the last H-bond in helix D, respectively. If large calcium-induced changes in the exchange rates occur in small isolated regions, rather than in continuous segments, a possible explanation is a change in interhelix angles on calcium binding. Such a motion would require only subtle conformational changes near the centers of the helices even if the ends of the helices move substantially. Studies of troponin C show that the interhelix angle within an EF-hand may increase when $Ca^{2+}$ is released (Herzberg et al., 1985, 1986). In addition, Skelton et al. (1989) have shown, on the basis of sequential and medium-range NOE's, that apo calbindin contains the same four helices as the $Ca_2$ form, at least at pH 5.6. Changes in exchange rates of helix amide protons may thus be caused by increased dynamics following changes in helix packing.

Since the solution conformation of the $Ca^{2+}$-loaded calbindin is probably highly similar to the crystal structure (Kördel et al., 1989), we have used the crystal structure (Szebenyi & Moffat, 1986) for mapping the regions where calcium removal highly affects NH exchange rates. It is evident from a stereo view (Figure 7A) that not only the $Ca^{2+}$-binding region but also the opposite end of the protein is affected. In addition, there appears to be large effects of $Ca^{2+}$ release throughout helix B. Residues have been grouped into two categories depending on whether the NH exchange in the apo form is fast ($k > 10^{-2}\ s^{-1}$, black symbol) or slow ($k < 10^{-2}\ s^{-1}$, gray symbol). The latter category probably contains residues for

Table II: Amide Hydrogens with Exchange Rates Increased More Than 3 Orders of Magnitude as a Result of $Ca^{2+}$ Removal

| NH | $\log k_{apo} - \log k_{Ca}$ | note |
|---|---|---|
| Glu60 | ≥5.0 | H-bonded to Ca ligand; carbonyl ligand in site II; likely side-chain ligand in site I |
| Ser24 | 4.9 | H-bonded to Ca ligand |
| Phe66 | 4.7 | Glu65 side chain is Ca ligand |
| Ile73 | 4.5 | |
| Leu28 | ≥4.1 | slow in apo |
| Leu32 | 3.6 | slow in apo |
| Gln22 | 3.6 | H-bonded to Ca ligand |
| Leu53 | ≥3.5 | Asp54 side chain is $Ca^{2+}$ ligand |
| Ala14 | 3.5 | carbonyl ligand in site I |
| Ser62 | 3.5 | H-bonded to Ca ligand |
| Asp58 | 3.5 | H-bonded to Ca ligand |
| Gln75 | 3.3 | |
| Leu39 | 3.3 | |
| Tyr13 | 3.2 | slow in apo |
| Glu5 | 3.0 | |
| Lys16 | 3.0 | |
| Leu31 | 3.0 | slow in apo |

which the effect of $Ca^{2+}$ removal results from an increased frequency of a global opening process. There are, on the other hand, a number of residues for which $Ca^{2+}$-induced effects on NH exchange rates are small ($\log k_{apo} - \log k_{Ca} < 1.4$) and for which the exchange in the apo form is slow ($\log k < -2$). As can be seen in Figure 7B, these residues are found primarily in the central part of calbindin. By comparison of panels A and B of Figure 7, it is clear that regions of large $Ca^{2+}$-induced effects, which lead to fast exchange in the apo form, are separated by a region of small effects where the exchange is slow also in the apo form. It thus seems possible that the large $Ca^{2+}$-induced retardation of NH exchange for Glu5, Ile73, Gln75, Leu39, and Leu40 is the result of a change in interhelix angles. This change might pertain to the average interhelix angles or the rate of large-scale fluctuations involving these angles. It should be kept in mind that the exchange rates found for many NH's in the C-terminal half are already in the $Ca^{2+}$ form within 2 orders of magnitude from that of a freely exposed peptide chain. There is thus no room for large increases in exchange rates, so that conformational changes are difficult to detect by measurement of effects on these rates.

*Val70.* Only for one NH proton, Val70, is the exchange significantly slower in apo calbindin as compared to the $Ca_2$ form. We note that there is a large pH dependence in the exchange rate of this amide proton. The quenching experiments using 2D NMR and the qualitative classification of NH exchange rates at pH 6.0 (Kördel et al., 1989) indicate that the exchange rate of the Val70 NH is lower than $10^{-3}$ $s^{-1}$ in the $Ca_2$ form. The exchange rate of this NH thus increases by more than a factor of $10^3$ as pH is raised from 6 to 7.5. From measurements of the pH dependence of chemical shifts, Dalgarno et al. (1983) have concluded that (de)ionization of the unblocked N-terminal amino group (with $pK_a \approx 8.0$) leads to a small alteration of the fold of $Ca_2$ calbindin in the region around Val70. This deformation may well involve a change in hydrogen bonding and/or solvent accessibility of the Val70 NH.

## Conclusions

The combined use of exchange-out, solvent saturation-transfer, and quenching experiments has made possible a detailed study of backbone amide proton exchange rates in calbindin $D_{9k}$ in both its calcium-loaded and its apo forms. The $Ca_2$ form appears to be very stable with a large proportion of the NH's exchanging slowly. There are significant effects of $Ca^2$ removal on the NH exchange rates throughout the entire protein, and the backbone dynamics in the apo form seem to involve larger segments, possibly the entire protein. Specific conclusions that could be drawn were (i) the β-sheet between the loops exists in both the $Ca_2$ and apo forms, (ii) hydrogen bonds involving backbone NH's within the loops (Lys16, Glu17, Asp58, Gly59, and Glu60) are broken or weakened after $Ca^{2+}$ removal, and (iii) $Ca^{2+}$ binding appears to induce a change in the interhelix angles and/or slows down the interhelix angle fluctuations. The present data can be used as a reference for evaluation of structural and dynamical consequences of site-specific mutations, binding of metal ions other than $Ca^{2+}$, and pH and temperature changes.

## Acknowledgments

We thank Peter Brodin and Eva Thulin for help with preparation of protein samples, CarlJohan Kördel and Walter J. Chazin for access to the assignments of $Ca_2$ calbindin prior to publication, Jane S. Richardson for drawing Figure 1, and Mats Lundell for drawing Figures 5 and 6. Valuable discussions with and helpful comments on the manuscript by Sture Forsén, Maria Selander, and Jannette Carey are gratefully acknowledged.

**Registry No.** Ca, 7440-70-2.

## References

Ahlström, P., Teleman, O., Kördel, J., Forsén, S., & Jönsson, B. (1989) *Biochemistry 28*, 3205–3211.

Benson, E. S., Fanelli, M. R. R., Giacometti, G. M., Rosenberg, A., & Antonini, E. (1972) *Biochemistry 12*, 2699–2706.

Brodin, P., Grundström, T., Hofmann, T., Drakenberg, T., Thulin, E., & Forsén, S. (1986) *Biochemistry 25*, 5371–5377.

Brodin, P., Drakenberg, T., Thulin, E., Forsén, S., & Grundström, T. (1989) *Protein Eng. 2*, 353–358.

Chazin, W. J., Kördel, J., Drakenberg, T., Thulin, E., Brodin, P., Grundström, T., & Forsén, S. (1989) *Proc. Natl. Acad. Sci. U.S.A. 86*, 2195–2198.

Dalgarno, D. C., Levine, B. A., Williams, R. J. P., Fullmer, C. S., & Wasserman, R. H. (1983) *Eur. J. Biochem. 137*, 523–529.

Drakenberg, T., Hofmann, T., & Chazin, W. J. (1989) *Biochemistry 28*, 5946–5954.

Forsén, S., & Hoffman, R. A. (1963) *Acta Chem. Scand. 17*, 1787–1788.

Haruyama, H., Qian, Y.-Q., & Wüthrich, K. (1989) *Biochemistry 28*, 4312–4317.

Herzberg, O., & James, M. N. G. (1985) *Nature 313*, 653–659.

Herzberg, O., Moult, J., & James, M. N. G. (1986) *J. Biol. Chem. 261*, 2638–2644.

Ikura, M., Minowa, O., & Hikichi, K. (1985) *Biochemistry 24*, 4264–4269.

Ikura, M., Minowa, O., Yagawa, M., Yagi, K., & Hickichi, K. (1987) *FEBS Lett. 219*, 17–21.

Johansson, C., Brodin, P., Grundström, T., Thulin, E., Forsén, S., & Drakenberg, T. (1990) *Eur. J. Biochem. 187*, 455–460.

Kördel, J., Forsén, S., & Chazin, W. J. (1989) *Biochemistry 28*, 7065–7074.

Kördel, J., Drakenberg, T., Forsén, S., & Chazin, W. J. *Biochemistry* (1990) (in press).

Kretsinger, R. H. (1980) *CRC Crit. Rev. Biochem. 8*, 119–174.

Kretsinger, R. H. (1987) *Cold Spring Harbor Symp. Quant. Biol. 52*, 499–510.

Kretsinger, R. H., & Nockolds, C. E. J. (1973) *J. Biol. Chem. 248*, 3313-3326.
Kuwajima, K., Kim, P. S., & Baldwin, R. L. (1983) *Biopolymers 22*, 59-67.
Lennick, M., & Allewell, N. M. (1981) *Proc. Natl. Acad. Sci. U.S.A. 78*, 6759-6763.
Linse, S., Brodin, P., Drakenberg, T., Thulin, E., Sellers, P., Elmdên, K., Grundström, T., & Forsén, S. (1987) *Biochemistry 26*, 6723-6735.
Molday, R., Englander, S. W., & Kallen, R. (1972) *Biochemistry 11*, 150-158.
O'Neil, J. D. J., & Sykes, B. D. (1988) *Biochemistry 27*, 2753-2762.
Pitner, T. P., Glickson, J. D., Dadok, J., & Marshall, G. R. (1974) *Nature 250*, 582.
Plateau, P., & Guéron, M. (1982) *J. Am. Chem. Soc. 104*, 7310-7311.
Qiwen, W., Kline, A. D., & Wüthrick, K. (1987) *Biochemistry 26*, 6488-6493.
Ramstein, J., Charlier, M., Maurizot, J. C., Szabo, A. G., & Hélène, C. (1979) *Biochem. Biophys. Res. Commun. 88*, 124-129.
Roder, H., Elöve, G., & Englander, S. W. (198) *Nature 335*, 700-704.
Seeholzer, S. H., & Wand, A. J. (1989) *Biochemistry 28*, 4011-4020.
Seeholzer, S. H., Cohn, M., Putkey, J. A., Means, A. R., & Crespi, H. L. (1986) *Proc. Natl. Acad. Sci. U.S.A. 83*, 3634-3638.
Skelton, N. J., Kördel, J., Forsén, S., & Chazin, W. J. (1990) *J. Mol. Biol.* (in press).
Szebenyi, D. M. E., & Moffat, K. (1986) *J. Biol. Chem. 261*, 8761-8777.
Teleman, O., & Jönsson, B. (1986) *J. Comp. Chem. 7*, 58-66.
Tsuda, S., Hasegawa, Y., Yoshida, M., Yagi, K., & Hikichi, K. (1988) *Biochemistry 27*, 4120-4126.
Tüchsen, E., & Woodward, C. (1985) *J. Mol. Biol. 185*, 405-419.
Tüchsen, E., & Woodward, C. (1987) *J. Mol. Biol. 193*, 793-802.
Udgaonkar, J. B., & Baldwin, R. L. (1988) *Nature 335*, 694-699.
Wagner, G. (1983) *Q. Rev. Biophys. 16*, 1-57.
Wand, A. J., Roder, H., & Englander, S. W. (1986) *Biochemistry 25*, 1107-1114.
Wendt, B., Hofmann, T., Martin, S. R., Bayley, P., Brodin, P., Grundström, T., Thulin, E., Linse, S., & Forsén, S. (1988) *Eur. J. Biochem. 175*, 439-445.
Woodward, C., Simon, I., & Tüchsen, E. (1982) *Mol. Cell. Biochem. 48*, 135-160.
Wüthrich, K., Strop, S., Ebina, S., & Williamson, M. P. (1984) *Biochem. Biophys. Res. Commun. 122*, 1174-1178.

# Effects of Spermidine and Hexaamminecobalt(III) on Thymine Imino Proton Exchange†

G. Eric Plum‡ and Victor A. Bloomfield*
*Department of Biochemistry, University of Minnesota, 1479 Gortner Avenue, St. Paul, Minnesota 55108*
*Received December 4, 1989; Revised Manuscript Received April 3, 1990*

ABSTRACT: We examine the influence of spermidine and hexaamminecobalt(III) binding on DNA base pair dynamics. Proton NMR line-width measurements are used to monitor the exchange of the thymine imino proton in poly[dA]·poly[dT] and in the alternating copolymer $[d(AT)]_{15}$·$[d(AT)]_{15}$. We employ the treatment by Benight et al. (1988) of diffusion effects in imino proton exchange to estimate catalytic rate constants and to extract apparent equilibrium constants for the interconversion between closed (nonexchanging) and solvent-accessible (exchangeable) states of the base pairs. The salt dependence of the spermidine-catalyzed imino proton exchange in poly[dA]·poly[dT] is qualitatively described by this theory. van't Hoff analysis of the temperature dependence of the apparent equilibrium constants suggests that the binding of spermidine and hexaamminecobalt(III) lowers the energy difference between the nonexchanging and exchanging states of the AT base pair in both duplexes.

Polyamines, as well as many other DNA binding molecules, stabilize the double helix against thermal denaturation (Mahler et al., 1961; Tabor, 1962). They may also promote alterations of the secondary structure of amenable sequences, the most profound being the transition between right-handed B-DNA and left-handed Z-DNA (Behe & Felsenfeld, 1981; Rich et al., 1984).

In addition to these major structural transitions, DNA undergoes a variety of subtle, small-scale alterations over the entire accessible temperature range (Palecek, 1976). These premelting transitions are observable by a number of techniques, particularly circular dichroism (Greve et al., 1977) and NMR (Patel, 1978).

Since polyamines and their analogues exhibit profound effects on the melting of double-stranded DNA, the question of their effects on other more subtle deformations of the DNA helix naturally follows. Well below the temperature where the DNA helix dissociates into two single-stranded polymers, transient disruptions of base pairing allow exchange with solvent of the imino protons of guanine and thymine (or uracil

†This research was supported by Research Grant GM 28093 from NIH and DMB 84-16305 from NSF.
*To whom correspondence should be addressed.
‡Present address: Department of Chemistry, Rutgers, The State University of New Jersey, Piscataway, NJ 08855-0939.

0006-2960/90/0429-5934$02.50/0 